# Nonlinear Regression Model of a Low-$g$ MEMS Accelerometer

Wei Tech Ang, *Member, IEEE*, Pradeep K. Khosla, *Fellow, IEEE*, and Cameron N. Riviere, *Member, IEEE*

***Abstract*—This paper proposes a nonlinear regression model of a microelectromechanical systems capacitive accelerometer, targeted to be used in tilt sensing and low-$g$ motion-tracking applications. The proposed model for the accelerometer's deterministic errors includes common physical parameters used to rate an accelerometer: scale factor, bias, and misalignment. Simple experiments used to reveal the behavior and characteristics of these parameters are described. A phenomenological modeling method is used to establish mathematical representations of these parameters in relation to errors such as nonlinearity and cross-axis effect, without requiring a complete understanding of the underlying physics. Tilt and motion-sensing experiments show that the proposed model reduces sensing errors to a level close to the residual stochastic noise.**

***Index Terms*—Accelerometer, error modeling, inertial sensing.**

## I. Introduction

ACCELEROMETERS have been used extensively in inclinometers to measure tilt and in inertial measurement units (IMUs) to measure acceleration. An inclinometer senses the direction of gravity and uses this information to determine the body tilt. A conventional six degrees-of-freedom IMU uses three accelerometers and three rate gyroscopes to sense a body's linear acceleration and angular velocity, and integrates these quantities with respect to time to give the instantaneous position and orientation of the body. There have been proposals for all-accelerometer IMU designs [1], [2] for cost-sensitive applications due to the superior performance of low-cost accelerometers relative to low-cost gyros [3]. In many recent low-$g$ ($< 2g$) inertial sensing applications, such as indoor robotic navigation [4], motion tracking of handheld devices for microsurgery [2], and entertainment [5], accelerometers have doubled as inclinometers to provide redundant orientation information.

With companies like Analog Devices leading the way, low-cost microelectromechanical systems (MEMS)-based accelerometers have gained substantial ground in inertial navigation applications in the past several years, especially in nonmilitary and consumer markets [6]–[8]. However, size and cost advantages notwithstanding, the performance of MEMS silicon accelerometers has not reached tactical or navigation grade. Testing of MEMS accelerometers on rolling artillery projectiles shows that they yield an average tracking error of about 0.1 $g$ throughout a 28-s test [9]. Though the report claims that such performance is acceptable, double integration of an acceleration error of 0.1 $g$ would mean a position error of more than 350 m at the end of the test.

It is because of this notorious integration drift that inertial measurement technology is seldom used alone in high-precision navigation or motion tracking applications. Any seemingly small error in the acceleration measurement would grow quadratically over time in the position measurement after the double integration. Therefore, to employ accelerometers effectively in high-precision tracking applications, it is imperative to obtain a comprehensive model to account for the errors.

There have been some efforts to model MEMS capacitive accelerometers using equivalent electrical circuit models that represent the physics of operation [10], [11]. However, the average user may find such models of limited benefit, since more useful parameters by which accelerometers are usually rated, such as scale factor, bias, nonlinearity, cross-axis sensitivity, and misalignment, are missing from these models.

The objective of this paper is to develop error models of low-$g$ MEMS accelerometers, by which the sensors can be compensated to improve accuracy. To model the nonlinear deterministic errors, we present a phenomenological modeling method that relates experimental observations to mathematical representations of parameters such as those mentioned above, without requiring complete understanding of the underlying physics. The proposed model thus identified is verified in tilt and motion sensing experiments where the ground truth is known. The limitations of the proposed model are also discussed. While the deterministic error model developed is specific to the make and model of accelerometer tested, the experiments and modeling methodology are general.

## II. Accelerometer Error Modeling

The sensor used in the development of the proposed physical model is the Analog Devices ADXL-203, a dual-axis low-$g$ miniature MEMS-based capacitive accelerometer. The ADXL-203 measures $5\times 5\times 2$ mm$^2$, weighs less than 1 g, and has an effective sensing range of $\pm 1.7$ $g$. It is a complete acceleration measurement system on a single monolithic integrated circuit. It contains a surface micromachined polysilicon structure built on top of a silicon wafer, with signal conditioning

Manuscript received November 11, 2005; revised August 20, 2006. This work was supported in part by the National Institutes of Health under Grant 1 R01 EB000526 and the National Science Foundation under Grant EEC-9731748. The associate editor coordinating the review of this paper and approving it for publication was Dr. Andre Bossche.

W. T. Ang is with the School of Mechanical and Aerospace Engineering, Nanyang Technological University, 639798 Singapore (e-mail: wtang@ntu.edu.sg).

P. K. Khosla is with the Department of Electrical Engineering and the Robotics Institute, Carnegie–Mellon University, Pittsburgh, PA 15213 USA (e-mail: pkk@ece.cmu.edu).

C. N. Riviere is with the Robotics Institute, Carnegie–Mellon University, Pittsburgh, PA 15213 USA (e-mail: camr@ri.cmu.edu).

Color versions of one or more of the figures in this paper are available online at http://ieeexplore.ieee.org.

Digital Object Identifier 10.1109/JSEN.2006.886995

1530-437X/$20.00 © 2006 IEEE

circuitry to implement an open-loop acceleration measurement architecture. Polysilicon springs at the four corners suspend the square proof mass over the surface of the wafer and provide a resistance against acceleration forces. The reader is referred to the datasheets and application notes from the manufacturer's Web site for more details.[1] The ADXL-203 provides two output modes: analog and digital pulse wave modulation (PWM). The former is used in our experiments, but the approaches described are also applicable to the latter.

Deterministic error refers to the error components that are related to the physics of the sensors' operation and their physical relationships with respect to one another and the environment, including geographic location. In the proposed model, we merely attempt to model the system response to an external excitation (i.e., acceleration) at the sensor level rather than at a component level that involves low-level circuitry and material properties.

### A. Scale Factor and Bias

Scale factor, sometimes referred to as sensitivity, is defined as the ratio of a change in the output to a change in the input intended to be measured. Bias or zero offset is the average sensor output over a specific time, measured at specified operating conditions, that has no correlation with the input. The scale factor and bias are affected by factors related to material and construction, e.g., hysteresis, nonlinearity, cross-axis effects, etc.

The scale factor of an accelerometer is usually expressed in volts per $g$ (V/$g$), where $g$ is the gravitational acceleration. Bias is expressed in volts or in terms of $g$ if the scale factor is known. To determine the scale factor and bias, the manufacturer specification sheets recommend the following:

$$\text{Scale factor} \quad \text{SF} = 1/2(V_{+g}V_{-g}) \quad \text{V}/g \tag{1}$$

$$\text{Bias} \quad B = 1/2(V_{+g} + V_{-g}) \quad \text{V} \tag{2}$$

where $V_{+g}$ and $V_{-g}$ are the voltage output of the accelerometer when aligned with the direction of gravity and opposite to the direction of gravity, respectively. Thus, with accelerometer output $V_o$, the sensed acceleration (in terms of $g$) is computed as

$$\text{Acceleration} \quad A = (V_o B)/\text{SF} \quad g. \tag{3}$$

However, the input–output relationship of the ADXL-203 accelerometer is nonlinear. The nonlinear behavior is a result of the material properties and the construction of the sensor. Two simple experiments will be performed to reveal the behavior of the accelerometer voltage output at orientations defined by two angles $\alpha$ and $\beta$, as depicted in Fig. 1. The angle $\alpha$ is defined to be 0° or 180° when the plane that contains both $x$- and $y$-sensing axes is perpendicular to the gravity plane (i.e., the vertical plane that contains the gravity vector) and ±90° is where the two planes are parallel. When $\alpha = 90°$, the angle $\beta$ is 0° when the $x$-accelerometer is aligned with the gravity vector.

In the first experiment, starting with $\alpha = 90°$ (see Fig. 2), we have the following.

[1]www.analog.com.

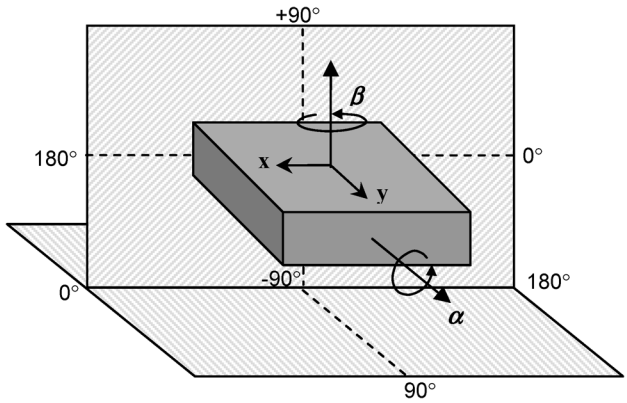


Fig. 1. Definition of angles $\alpha$ and $\beta$.

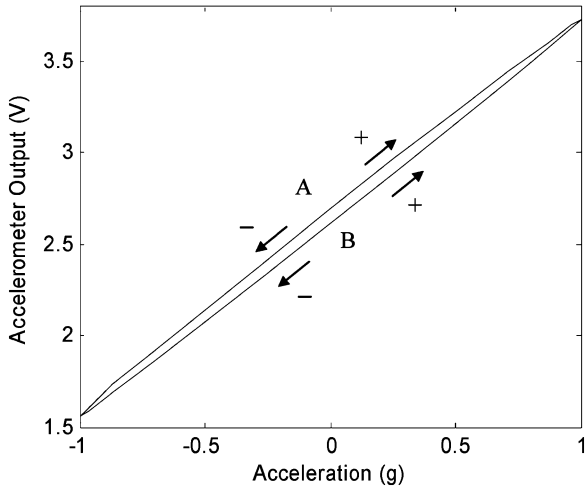


Fig. 2. Hysteresis-like paths of the accelerometer output when rotated in the gravity plane. When rotated first clockwise and then anticlockwise through 360°, it follows paths $\mathrm{A}^+ - \mathrm{B}^-$ and $\mathrm{B}^+ - \mathrm{A}^-$, respectively; when rotated first clockwise and then anticlockwise through 180° and back to 0°, it follows paths $\mathrm{A}^+ - \mathrm{A}^-$ and $\mathrm{B}^+ - \mathrm{B}^-$, respectively.

- When the accelerometer is rotated from $\beta = 0°$ to 360° clockwise and anticlockwise in the gravity plane, hysteresis-like paths $\mathrm{A}^+ - \mathrm{B}^-$ and $\mathrm{B}^+ - \mathrm{A}^-$, respectively, are observed.
- When it is rotated clockwise and anticlockwise from $\beta = 0°$ to 180° and then back to 0° in the gravity plane, paths $\mathrm{A}^+ - \mathrm{A}^-$ and $\mathrm{B}^+ - \mathrm{B}^-$, respectively, are observed.

In the second experiment, the accelerometer is inclined such that both the $x$- and $y$-sensing axes lie in a plane offset from the direction of gravity by the angle $\alpha$. The following is observed.

- When the accelerometer is rotated from $\beta = 0°$ to 360° in the inclined plane $\alpha$, there is a nonparallel upward shift of the entire hysteresis-like path with increasing $\alpha$.
- Experiments at $\pm\alpha$ yield the same hysteretic paths.

There is no change in the accelerometer output at $\alpha = 0°$ and 180°, since the sensing plane is orthogonal to gravity. For ease of illustration, only $Z_{\pm 30}$, $Z_{\pm 90}$, and $Z_{\pm 150}$ are shown in Fig. 3. Note that $Z_{\pm 90}$ is the same as in Fig. 2.

These observations are the result of composite nonlinearity errors, including material nonlinearity, hysteresis, and cross-axis effects. It is almost impossible to distinguish the

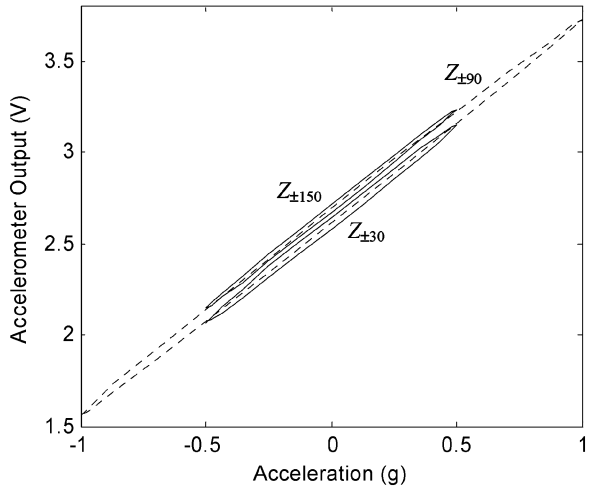


Fig. 3. Hysteresis-like paths of the accelerometer rotated through 360° in a plane inclined at angle $\alpha = \pm 30°, \pm 90°$, and $\pm 150°$.

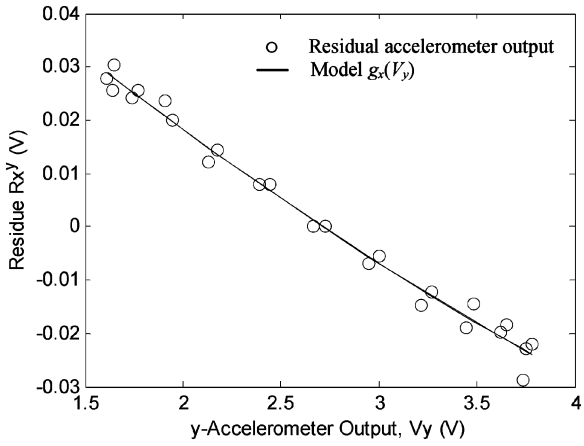


Fig. 4. The residual $x$-accelerometer output versus the $y$-accelerometer output. The relationship may be described by a quadratic function.

contributions of these several factors without specialized instrumentation. However, it is not necessary to understand the underlying physics, nor to model these errors explicitly; there is sufficient information for us to model and compensate these errors phenomenologically.

The hysteresis-like behavior of the ADXL-203 accelerometer is different from the classical hysteresis found in magnetism and other shape memory alloys. One possible explanation of this observation is the cross-axis effect from the acceleration in the $y$-axis. This is evident from the fact that, since accelerations in $x$- and $y$-sensing directions are 90° out of phase, the error of the $x$-axis is largest at the point where the $y$-direction acceleration is the largest, and vice versa.

One probable cause of the shift of the entire hysteresis path at different inclinations $\alpha$ is the out-of-plane cross-axis effect from the acceleration in the $z$-direction. This is again evident from the fact that the hysteretic curves shift upward as the out-of-plane $z$-axis acceleration increases.

Thus, the acceleration sensed by the $x$-accelerometer is the combined effect of the real acceleration in the $x$-axis plus cross-axis accelerations from the other two orthogonal principal directions, which alter the bias and the scale factor

$$A_x = (V_x B_x(V_y, V_z))/\mathrm{SF}_x(V_z) \tag{4}$$

where $V_y$ and $V_z$ are, respectively, the output of the $y$-accelerometer and an external $z$-accelerometer. It may seem strange to include a $z$-accelerator output term for a dual axis accelerometer with only $x$- and $y$-sensing, but in most motion tracking applications, the IMU has three orthogonal axes of linear acceleration sensing. In a static tilt sensing application, $z$-accelerator output can be calculated from simple vector geometry, since the only sensed acceleration is the gravity

$$V_z = V_g^z \sqrt{1 - \widetilde{V}_x^2 - \widetilde{V}_y^2} \tag{5}$$

where $\widetilde{V}_x$ and $\widetilde{V}_y$ are normalized voltages given by

$$\widetilde{V}_x = \frac{V_x}{V_g^x}, \widetilde{V}_y = \frac{V_y}{V_g^y} \tag{6}$$

and

$$V_g^d = \frac{1}{2}\left(V_{+g}^d - V_{-g}^d\right), d = x, y, \text{or } z \tag{7}$$

is the output of the $x$-, $y$-, or $z$-accelerometer in volts when aligned with gravity.

We first define a linear model $f_x(A_x)$ by rearranging (3)

$$f_x(A_x) = A_x \cdot \mathrm{SF}_x^{90} + B_x^{90} \tag{8}$$

where $\mathrm{SF}_x^{90}$ and $B_x^{90}$ are the scale factor and bias obtained from the manufacturer's recommended calibration method. The superscript "90" signifies $\alpha = 90°$.

The shift in bias is a linear superposition of the cross-axis effects from the $y$- and $z$-acceleration

$$B_x(V_y, V_z) = B_x^{90} + g_x(V_y) + h_x(V_z). \tag{9}$$

To model $g_x(V_y)$, the corresponding data generated by the linear model $f_x(A_x)$ are subtracted from the measurement data of plot $Z_{\pm 90}$ (where $h_x(V_z) = 0$)

$$R_x^y = V_{ox} - V_x \tag{10}$$

where $R_x^y$ is the residual $x$-accelerometer output attributed to the effect of acceleration in $y$-direction, $V_{ox}$ is the measured x-accelerometer output, and $V_x$ is the data generated by the linear model $f_x(A_x)$. $R_x^y$, $V_{ox}$, and $V_x$ are all $n \times 1$ vectors, where $n$ is the number of data points. Plotting the residue vector versus the measured $y$-accelerometer output vector reveals that the relationship may be described by a quadratic function (see Fig. 4). Hence the cross-axis effect of $y$-acceleration on the $x$-axis may be modeled by the least squares fitting of a second-order polynomial to the data

$$g_x(V_y) = p_{x2} V_y^2 + p_{x1} V_y + p_{x0}. \tag{11}$$

The result of this model is shown in Fig. 5.

To model $h_x(V_z)$, we first compute the bias of the hysteretic paths generated at each inclined plane using (2) and then the

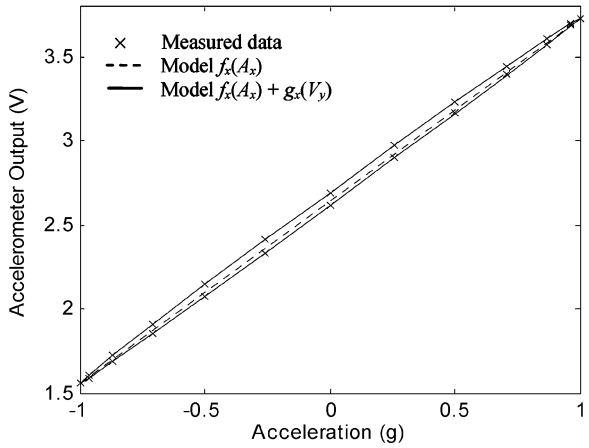


Fig. 5. The measured $x$-accelerometer output, the linear model $f_x(A_x)$, and the model $f_x(A_x) + g_x(V_y)$.

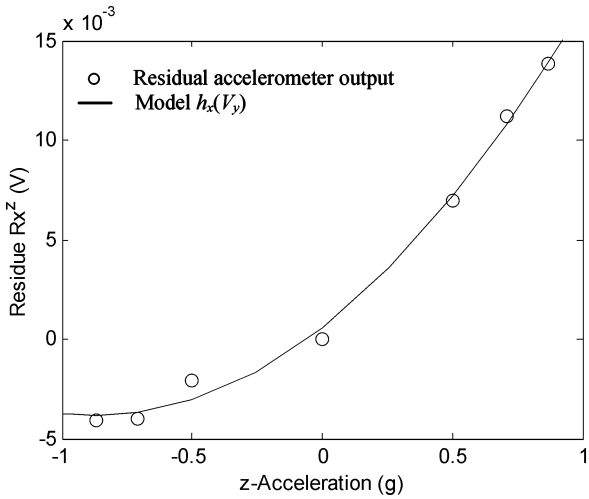


Fig. 6. The residual x-accelerometer output versus the $z$-acceleration. The relationship is quadratic.

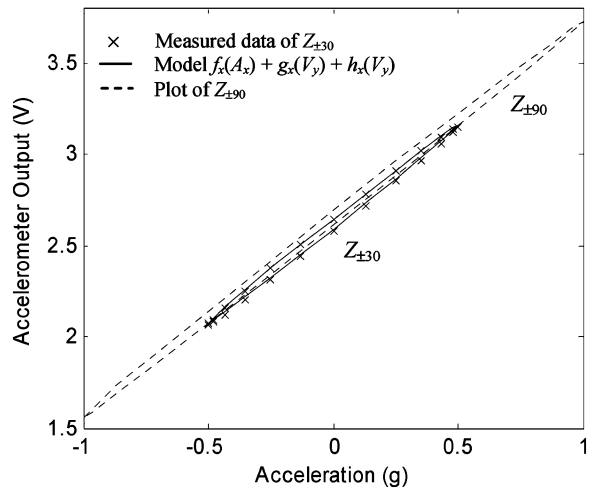


Fig. 7. The measured $x$-accelerometer output at $\alpha = \pm 30^\circ$ and the proposed physical model $f_x(A_x) + g_x(V_y) + h_x(V_z)$. The $Z_{\pm 90}$ plot is added for comparison.

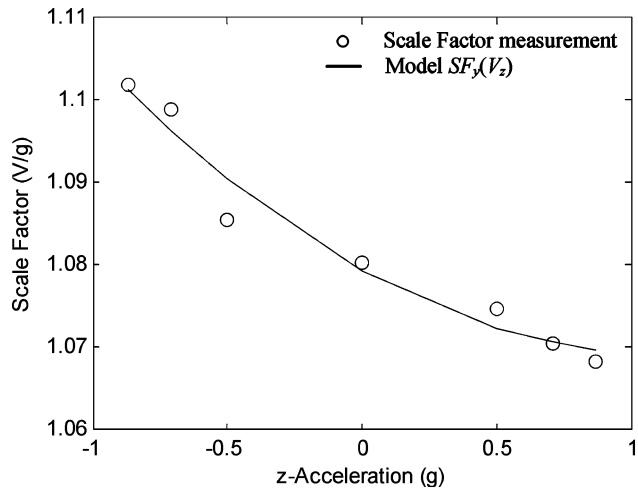


Fig. 8. Scale factor versus $z$-acceleration. The relationship is quadratic.

difference of the bias at each $\alpha$ compared with that at $\alpha = 90^\circ$. Thus

$$R_x^z = B_x^\alpha - B_x^{90} \tag{12}$$

where $R_x^z$ is the residual $x$-accelerometer output attributed to the effect of acceleration in $z$-direction, $B_x^\alpha$ is the vector of the bias at each $\alpha$, and $B_x^{90}$ contains repeated values of the bias at $\alpha = 90^\circ$. These are all $m \times 1$ vectors, where $m$ is the number of inclined planes in which we have conducted the experiment. Plotting $R_x^z$ versus the $z$-accelerometer output [in this case, an analytical result based on (5) is used] shows that the relationship is quadratic as shown in Fig. 6. Hence the cross-axis effect of $z$-acceleration on sensing in the $x$-axis may be modeled by a least squares fit of a second-order polynomial to the data

$$h_x(V_z) = q_{x2}V_z^2 + q_{x2}V_z + q_{x0}. \tag{13}$$

The result of this model is shown in Fig. 7.

Now we substitute (8), (11), and (13) into (4)

$$A_x = \big(V_x - B_x^{90} - p_{x2}V_y^2 - p_{x1}V_y - p_{x0} - q_{x2}V_z^2 - q_{x1}V_z - q_{x0}\big)/\mathrm{SF}_x(V_z) \tag{14}$$

where $\mathrm{SF}_x(V_z)$ is found from the plot of $\mathrm{SF}_x$ versus the $z$-acceleration $V_z$ as shown in Fig. 8. The scale factor model is thus

$$\mathrm{SF}_x(V_z) = r_{x2}V_z^2 + r_{x1}V_z + r_{x0}. \tag{15}$$

The same approach is repeated to model the $y$-sensing axis

$$A_y = \big(V_y - B_y^{90} - p_{y2}V_x^2 - p_{y1}V_x - p_{y0} - q_{y2}V_z^2 - q_{y1}V_z - q_{y0}\big)/\mathrm{SF}_y(V_z) \tag{16}$$

where

$$\mathrm{SF}_y(V_z) = r_{y2}V_z^2 + r_{y1}V_z + r_{y0}. \tag{17}$$

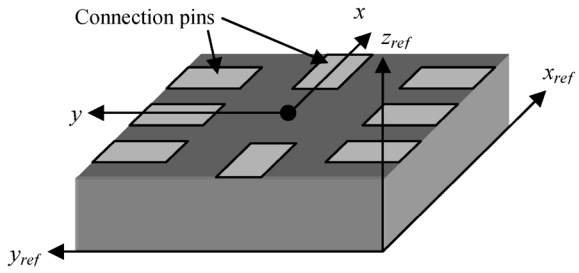


Fig. 9. Reference surfaces used to define misalignment of sensing axes.

### B. Misalignment

To model the misalignment errors, we select two reference surfaces or edges of the accelerometer and assume that the corresponding matching surfaces on the mounting structure are machined to a good tolerance. We then model the system-level misalignment errors of the sensing axes with respect to these two reference surfaces or edges. The flat square surface without the connection pins and one of the sides parallel to the $x$-sensing axis are chosen to be the references. We define the normal to the reference surface as $z_{\rm ref}$, the reference edge as $x_{\rm ref}$, and $y_{\rm ref}$ as the imaginary vector that completes the right hand coordinate system. The accelerometer is mounted with the reference surface aligned with the gravity plane and the reference edge parallel to the gravity vector. We rotate the accelerometer about $y_{\rm ref}$ by $\alpha$ and then about $z_{\rm ref}$ by $\beta$ until a maximum (or minimum if $x_{\rm ref}$ is aligned with $-g$) $x$-output voltage is registered. The orientation of the real $x$-sensing axis with respect to the reference frame $xyz_{\rm ref}$ is then found by

$$\Theta_x = R_y(\alpha_x)R_z(\beta_x)x_{\rm ref} = [\theta_{xx} \quad \theta_{xy} \quad \theta_{xz}]^T \tag{18}$$

where $R_y(\alpha_x)$ and $R_z(\beta_x)$ are 3×3 matrices representing rotation about $y_{\rm ref}$ and $z_{\rm ref}$, respectively, with $x_{\rm ref} = [0\ 0\ 1]^T$. For the $y$-sensing axis, we rotate the accelerometer by 90° about $z_{\rm ref}$ and repeat the same experiment to find $\alpha_y$ and $\beta_y$; then with $y_{\rm ref} = [0\ 1\ 0]^T$

$$\Theta_y = R_x(\alpha_y)R_z(\beta_y)y_{\rm ref} = [\theta_{yx} \quad \theta_{yy} \quad \theta_{yz}]^T. \tag{19}$$

The $x$- and $y$-accelerations obtained from (14)–(17) are sensed along directions $\Theta_x$ and $\Theta_y$, respectively. The accelerations along the reference axes may be computed as

$$A_{xref} \approx \frac{A_x - \theta_{xy}A_y - \theta_{xz}A_z}{\theta_{xx}} \tag{20}$$

$$A_{yref} \approx \frac{A_y - \theta_{yx}A_{xref} - \theta_{yz}A_z}{\theta_{yy}}. \tag{21}$$

Note that (20) uses uncorrected $A_y$ and $A_z$, while (21) uses the corrected $A_{x\rm ref}$ and uncorrected $A_z$. This would be a good approximation since the angles $\theta_{ij}$ are typically small when $i \neq j$. In our experiment, the parameters are found to be $\alpha_x = 0.75°$, $\beta_x = -0.33°$, $\Theta_x = [0.9999\ -0.0058\ -0.0131]^T$ and $\alpha_y = 0.75°$, $\beta_y = 0.5°$, $\Theta_y = [-0.0029\ 0.9999\ 0.0131]^T$. The $\alpha$s and $\beta$s are measured to an accuracy of $\pm 0.2°$.

### C. Tilt Sensing Experiment

*1) Experimental Setup:* All the experiments described in the previous sections are performed on an experimental setup made of two orthogonal precision rotary stages with resolution of 0.083° (5 arcmin). Each of the analog outputs ($x$ and $y$) is connected to the signal ground by a 0.33 $\mu$F capacitor, which combines with the sensor output impedance of 32 k$\Omega$ to become a simple first-order R–C low-pass filter with cutoff frequency at around 15.2 Hz. The sensor output is sampled at 1 kHz by a 16-bit analog-to-digital converter. The inclinations of the rotary stages are checked prior to each experiment by a digital level with a resolution of 0.1°. The noise floor of the sensor analog outputs is about 3.1 mV p-p, which is computed from four times the measured root mean square (rms) noise, the upper limit of the peak-to-peak noise 95.4% of the time, as specified in the datasheet. This would correspond to a minimum perceivable inclination change of approximately 0.2°. This means that experimental errors due to human inconsistency and parallax error on the order of 0.01° are negligible compared to the noise floor. Because of the stochastic nature of the sensor output, the mean of 5 s worth of data (5000 data points) is used in these experiments.

*2) Results:* Fig. 10(a)–(c) shows the errors in tilt estimation of the accelerometers with the proposed physical model and with the manufacturer recommended linear model. In Fig. 10(a), $\beta$ is held constant at 0° while $\alpha$ is rotated from −180° to 180° at 30° intervals. In Fig. 10(b), $\alpha$ is held constant at 0° while $\beta$ is rotated from −180° to 180° at 30° intervals. In Fig. 10(c), $\alpha$ and $\beta$ are rotated simultaneously from −180° to 180° at 30° intervals. In all three experiments, the proposed model consistently outperforms the manufacturer recommended linear model in both rms error (rmse) and maximum error of estimating the tilt angles. The numerical results of the experiment are summarized in Table I.

### D. Discussion

The proposed nonlinear model for the deterministic errors has performed well compared to the manufacturer's recommended linear model as described by (3) in both tilt sensing and motion sensing experiments. In the motion sensing experiment, the rmse is 20.8 mm/s$^2$. The rated rms noise of the ADXL-203 accelerometer when bandlimited to 15.2 Hz is 16.4 mm/s$^2$ (computed from rated noise density of 110 $\mu$g/$\sqrt{\rm Hz}$ rms). This is comparable to the experimental value reported above. This means that our model has successfully reduced sensing errors almost to the level of residual stochastic noise.

### E. Motion Sensing Experiment

*1) Experimental Setup:* The motion sensing experiment consists of a motion generator and a displacement sensor. The motion generator is a three-axis piezodriven linear nanopositioner (Polytec-PI, Inc., Model P-611) and the motion sensor is an infrared interferometer (Philtec, Inc., Model D63) with submicrometer resolution. An ADXL-203 accelerometer is mounted on top of the motion generator with its reference edges aligned with the edges of the motion generator. The motion generator is mounted on the rotary stages with an inclination of $\alpha = +45°$ and rotated to $\beta = +90°$, as shown in Fig. 11. The motion generator generates an oscillation of 60 $\mu$m p-p at 10 Hz in the $x$-sensing direction, which is perpendicular to the gravity vector. The interferometer is placed in front of the motion generator aligned with the $x$-direction to measure the displacement

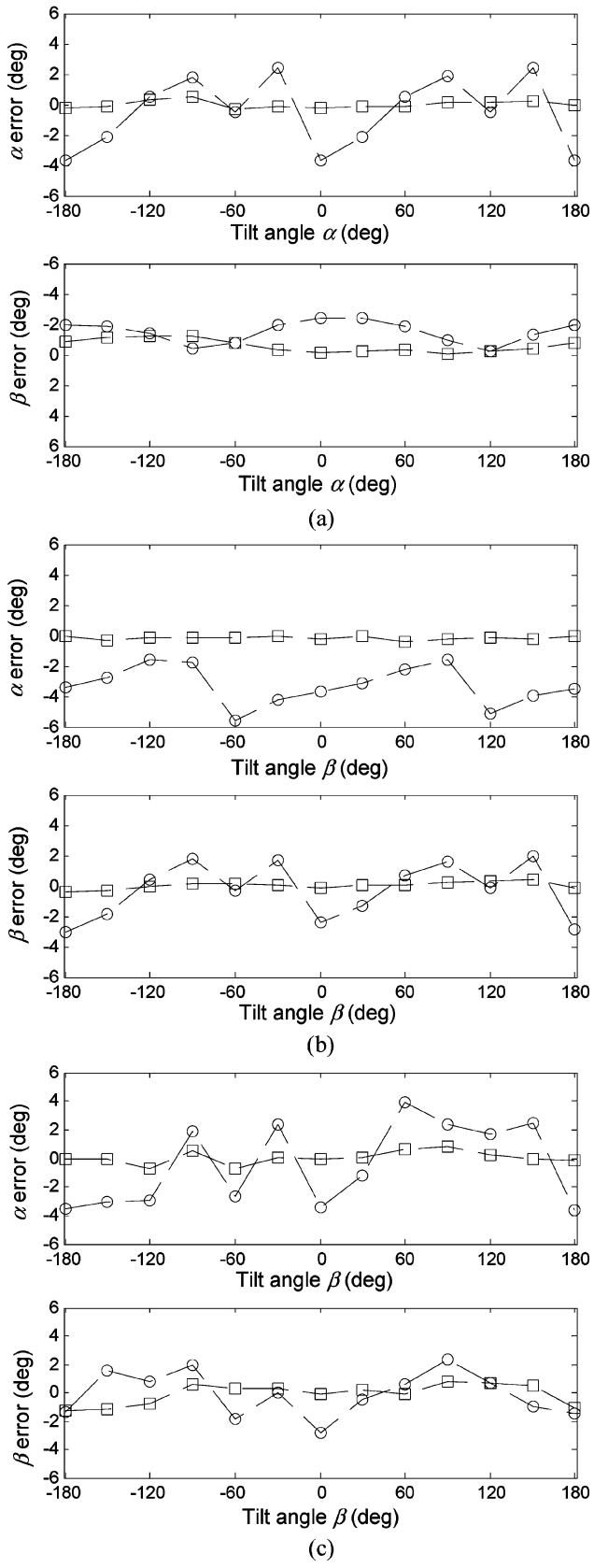


Fig. 10. Errors in tilt angle estimation using the proposed physical model and the manufacturer's recommended linear model. (a) $\beta = 0°$ and $\alpha$ is rotated from $-180°$ to $180°$ at $30°$ intervals. (b) $\alpha = 0°$ and $\beta$ is rotated from $-180°$ to $180°$ at $30°$ intervals. (c) $\alpha$ and $\beta$ are rotated simultaneously from $-180°$ to $180°$ at $30°$ intervals.

TABLE I
RMSE AND MAXIMUM ERROR OF THE TILT ESTIMATION EXPERIMENTS

| | Tilt angle $\alpha$ | | | Tilt angle $\beta$ | | |
|---|---|---|---|---|---|---|
| | Linear Model | Physical Model | % reduction | Linear Model | Physical Model | % reduction |
| Rmse (deg) | 2.88 | 0.32 | 88.9 | 1.64 | 0.60 | 63.4 |
| Max err (deg) | 3.95 | 0.82 | 79.2 | 2.36 | 0.82 | 65.3 |

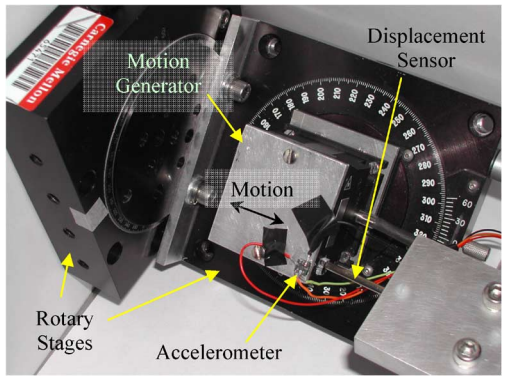


Fig. 11. Motion sensing experiment setup.

profile of the motion generator. The interferometer is sampled at 1 kHz.

*2) Results:* The data collected by the interferometer are low-pass filtered with a second-order digital Butterworth filter with cutoff frequency at 20 Hz. It is then corrected for phase shift and attenuation before being differentiated twice to obtain the acceleration profile of the motion generator. The accelerometer voltage output is also corrected for phase shift and attenuation due to the analog R–C low-pass filter and then converted to acceleration in mm/s$^2$ based on both the manufacturer's recommended linear model (1)–(3) and the proposed nonlinear model (4)–(21). The gravity constant $g$ used is 9801.31 mm/s$^2$, computed based on the latitude and altitude of our laboratory.

Fig. 12(a) shows the acceleration profile sensed by the interferometer and that based on the linear model. The rmse is 299.8 mm/s$^2$, most of which is the result of the shift in bias. Fig. 12(b) shows the same interferometer acceleration plot and that computed by the proposed physical model. The proposed nonlinear regression model eliminates most of the bias shift error. The rmse is 20.8 mm/s$^2$, an improvement of 93.1% over the linear model.

The action of each component of the proposed model is depicted in Fig. 13. The accelerometer is first calibrated at $\alpha = +90°$, which gives the line labeled "Linear Model." For the motion sensing experiment, the accelerometer is rotated to $\alpha = +45°$ and $\beta = +90°$ at which its response to acceleration in the $x$-direction is represented by the line labeled "Actual Response." With the output voltage $V_x$, the linear model indicates an acceleration of $A'_x$. The difference between the actual acceleration $A_x$ and $A'_x$ results in the offset observed in Fig. 12(a). The model $B_x(V_y, V_z)$ shifts the linear model parallel toward the actual response; and the model $\mathrm{SF}_x(V_z)$ alters the gradient

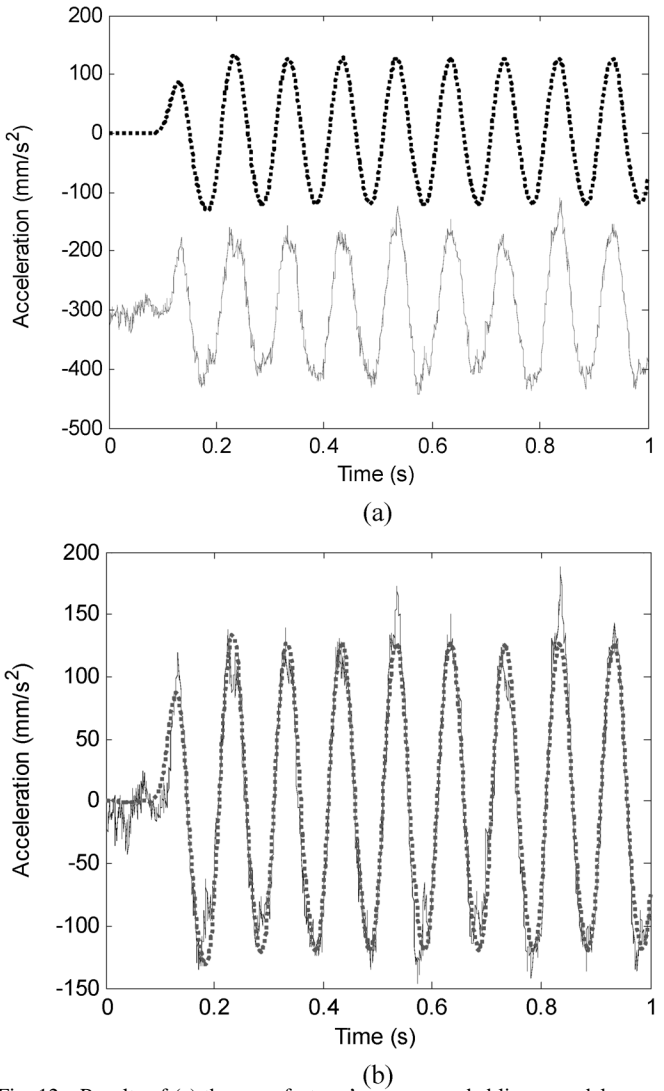


Fig. 12. Results of (a) the manufacturer's recommended linear model versus (b) the proposed nonlinear model. The dotted line is the computed acceleration from the interferometer. The solid line is the measured acceleration from the $x$-accelerometer.

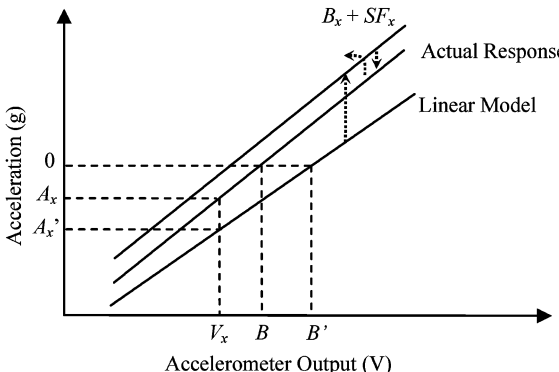


Fig. 13. Action of each component of the proposed nonlinear regression model on the accelerometer response plot. The line "Linear Model" is obtained from the manufacturer's recommended calibration method. The bias model $B_x(V_y, V_z)$ shifts the linear model parallel towards the actual response and the model $\mathrm{SF}_x(V_z)$ alters the gradient and result in the line "$B_x + \mathrm{SF}_x$." The misalignment model makes the final shift to the line "Actual Response."

and result in the line "$B_x + \mathrm{SF}_x$." Correction for the misalignment vector $\Theta_x$ makes the final shift of the line toward the actual response, which gives the plot in Fig. 12(b). The strength of this phenomenological approach of modeling the scale factor, bias, and misalignment is that errors such as nonlinearity and cross-axis effects are captured with very simple experiments without the need to understand the underlying physics.

## III. Conclusion

A nonlinear regression model for the deterministic errors of a dual-axis MEMS accelerometer intended for low-$g$ applications has been proposed. The model is based on phenomenological modeling of the physical parameters by which an accelerometer is commonly rated: scale factor, bias, and misalignment. In tilt and motion sensing experiments, the proposed model reduces sensing error almost to the level of stochastic noise.

## Acknowledgment

The authors would like to thank S. Khoo for his assistance in conducting the experiments.

## References

[1] J. H. Chen, S. C. Lee, and D. B. DeBra, "Gyroscope free strapdown inertial measurement unit by six linear accelerometers," *J. Guid., Contr., Dyn.*, vol. 17, no. 2, pp. 286–290, Mar.–Apr. 1994.

[2] W. T. Ang, P. K. Khosla, and C. N. Riviere, "Design of all-accelerometer inertial measurement unit for tremor sensing in handheld microsurgical instrument," in *Proc. IEEE Int. Conf. Robot. Automat.*, Sep. 2003, pp. 1781–1786.

[3] C.-W. Tan, A. Park, K. Mostov, and P. Varaiya, "Design of gyroscope-free navigation systems," in *Proc. IEEE Intell. Transport. Syst. Conf.*, Aug. 2001, pp. 286–291.

[4] B. Barshan and H.F. Durrant-Whyte, "Inertial navigation systems for mobile robots," *IEEE Trans. Robot. Automat.*, vol. 11, pp. 328–342, Feb. 1994.

[5] X. Yun, M. Lizarraga, E. R. Bachmann, and R. B. McGhee, "An improved quaternion-based kalman filter for real-time tracking of rigid body orientation," in *Proc. IEEE/RSJ Int. Conf. Intell. Robot. Syst.*, Las Vegas, NV, Oct. 2003, pp. 1074–1079.

[6] N. Barbour and G. Schmidt, "Inertial sensor technology trends," *IEEE Sensors J.*, vol. 1, no. 4, pp. 332–339, Dec. 2001.

[7] J. L. Weston and D. H. Titterton, "Modern inertial navigation technology and its application," *Electron. Commun. Eng. J.*, pp. 49–64, Apr. 2000.

[8] C. Verplaetse, "Inertial proprioceptive devices: self-motion-sensing toys and tools," *IBM Syst. J.*, vol. 35, no. 3&4, pp. 639–650, 1996.

[9] B. S. Davis, "Using low-cost mems accelerometers and gyroscopes as strapdown IMUs on rolling projectiles," in *Proc. Position Location Navig. Symp.*, Apr. 1998, pp. 594–601.

[10] W. F. Lee, P. K. Chan, and L. Siek, "Electrical modeling of MEMS sensors for integrated accelerometer applications," *Proc. Electron Devices Meet.*, pp. 88–91, Jun. 1999.

[11] C. Bourgeois, F. Porrent, and A. Hoogerwerf, "Analytical modeling of squeeze-film damping in accelerometers," in *Proc. IEEE Int. Conf. Solid-State Sens. Actuators*, Jun. 1997, pp. 1117–1120.

**Wei Tech Ang** (S'98–M'04) received the B.Eng. and M.Eng. degrees in mechanical and production engineering from Nanyang Technological University, Singapore, in 1997 and 1999, respectively, and the Ph.D. degree in robotics from Carnegie–Mellon University, Pittsburgh, PA, in 2004.

He has been an Assistant Professor in the School of Mechanical and Aerospace Engineering, Nanyang Technological University, since 2004. His research interests include sensing and sensor, medical robotics, rehabilitative and assistive technology, mechanism design, kinematics, signal processing, and learning algorithms.

**Pradeep K. Khosla** (F'95) received the B.Tech. degree (honors) from IIT, Kharagpur, India, and the M.S. and Ph.D. degrees from Carnegie–Mellon University, Pittsburgh, PA, in 1984 and 1986, respectively.

He was an Assistant Professor of electrical and computer engineering and robotics at Carnegie–Mellon University from 1986 to 1990, Associate Professor from 1990 to 1994, Professor since 1994, and Founding Director of the Institute for Complex Engineering from 1997 to 1999. He is currently the Philip and Marsha Dowd Professor of Engineering and Robotics and Head of the Electrical and Computer Engineering Department. From January 1994 to August 1996, he was a DARPA Program Manager. His research interests are in the areas of Internet-enabled collaborative design and distributed manufacturing, agent-based architectures for distributed design and embedded control, software composition and reconfigurable software for real-time embedded systems, and reconfigurable and distributed robotic systems. His research has resulted in two books and more than 200 journal articles, conference papers, and book contributions. He is currently an Associate Editor of the *Journal of Computers and Information Science in Engineering*.

Prof. Khosla received the Carnegie Institute of Technology Ladd Award for excellence in research in 1989, the ASEE 1999 George Westinghouse Award for Education, the Siliconindia Leadership award for Excellence in Academics and Technology in 2000, and the W. Wallace McDowell award from the IEEE Computer Society in 2001. He became a Distinguished Lecturer for the IEEE Robotics and Automation Society for 1998–2001. He was General Chairman for the 1990 IEEE International Conference on Systems Engineering, Program Vice Chairman of the 1993 International Conference on Robotics and Automation, General Cochairman of the 1995 Intelligent Robotics Systems conference, and Program Vice-Chair for the 1997 IEEE Robotics and Automation Conference. He was Technical Editor of the IEEE TRANSACTIONS ON ROBOTICS AND AUTOMATION.

**Cameron N. Riviere** (S'94–M'96) received the B.S. degree in aerospace engineering and ocean engineering from the Virginia Polytechnic Institute and State University, Blacksburg, in 1989 and the Ph.D. degree in mechanical engineering from The Johns Hopkins University, Baltimore, MD, in 1995.

Since 1995, he has been with the Robotics Institute, Carnegie–Mellon University, Pittsburgh, PA, where he is presently an Associate Research Professor. His research interests include medical robotics, control systems, signal processing, learning algorithms, and biomedical applications of human–machine interfaces.